ARTICLE IN PRESS

Mechanism and Machine Theory xxx (2009) xxx–xxx

Contents lists available at ScienceDirect

Mechanism and Machine Theory

journal homepage: www.elsevier.com/locate/mechmt

Cheope: A new reconfigurable redundant manipulator

D. Tosi [a], G. Legnani [a,*], N. Pedrocchi [b], P. Righettini [c], H. Giberti [d]

[a] Dip. Ing. Meccanica e Industriale, Università di Brescia, Italy
[b] ITIA-CNR, Istituto Tecnologie Industriali e Automazione, Consiglio Nazionale Ricerche, Milano, Italy
[c] Dip. di Progettazione e Tecnologie, Università di Bergamo, Italy
[d] Dip. di Meccanica, Politecnico di Milano, Italy

ARTICLE INFO

Article history:
Received 5 July 2006
Received in revised form 31 July 2009
Accepted 18 November 2009
Available online xxxx

Keywords:
Parallel manipulator
Redundant manipulator
Reconfigurable manipulator
Singularity
Workspace

ABSTRACT

This work presents a new reconfigurable parallel-serial hybrid manipulator that can reach 7 degrees of freedom as a whole. The architecture of the parallel part is modular and it can be configured to obtain for the mobile base 3 or 4 degrees of freedom, or 3 degrees of freedom with redundant actuation. The paper presents the new parallel kinematic structure, analyzing the singularities, the workspace and the benefits of the redundant configuration. Finally, the first experimental results are presented.

1. Introduction

Robotic aid for surgeons is a new and burgeoning manipulator application field because of the great accuracy and dexterity that can now be guaranteed by robots at the end-effector. Many prototypes of medical robots have been developed and some commercial products can be found (Da Vinci [1], Zeus [2], etc.). In the context of the RIME project (Robot In Medical Environment), the Mechanical Engineering Department of the Università degli Studi di Brescia, in cooperation with the Politecnico di Milano, has designed and constructed a robot manipulator for intervertebral pedicle screw implantation in spinal surgery [3]. The robot arm is used here in the critical phase of execution of small holes in adjacent vertebras in which the screws needed to fix a bracing plate to the spine are manually inserted. The task specifications in orthopedic machining are high stiffness, great accuracy and a life-safety reaction at unexpected or dangerous events. Parallel architecture is a feasible design solution: 6 degree of freedom (dof) parallel manipulators provide high stiffness but are generally extremely complex [4]. Parallel Kinematic Machines (PKMs) with less than 6 dof [5,13] are instead simpler in design, but often limited in dexterity. A common solution to enhance the dexterity of a PKM is the development of a hybrid architecture [6–9].

Cheope, the prototype presented here, is a parallel-serial hybrid manipulator with a parallel structure that carries a serial chain which includes a wrist. The parallel part is similar to the one of the manipulator described in [10]. However the link disposition is different and Cheope structure is modular: its architecture can be modified with simple and fast mechanical operations to obtain different mobility configurations with 3 or 4 dof. The serial part is a small serial chain (wrist) carried by the mobile base (platform) of the parallel architecture. It allows the end-effector a wide range of rotation. The design of the

* Corresponding author. Address: Università di Brescia, Dip. Ing. Meccanica, via Branze 38, 25123 Brescia, Italy. Tel.: +39 030 3715 425; fax: +39 030 3702 448.
E-mail address: giovanni.legnani@ing.unibs.it (G. Legnani).

0094-114X/$ - see front matter © 2009 Elsevier Ltd. All rights reserved.
doi:10.1016/j.mechmachtheory.2009.11.005

Please cite this article in press as: D. Tosi et al., Cheope: A new reconfigurable redundant manipulator, Mech. Mach. Theory (2009), doi:10.1016/j.mechmachtheory.2009.11.005

manipulator has been optimized to exploit the advantages of both kinematic architectures, avoid singularities and supply an isotropic behavior in the center of the workspace [9].

This optimized design and the high performance of its components make Cheope parallel structure suitable for other fields of application such as fast pick and place, machining, and assembly tasks by simply changing the serial part.

In Sections 2 and 3 we introduce the reconfigurable topology of the Cheope parallel structure and develop a kinematic analysis of its main configurations. The kinematic and constraint singularities are studied in Section 4, analyzing the Jacobian matrix and following the method proposed by Zoppi [16]. Section 5 describes and verifies the conditions for backlash compensation in the redundant configuration. In Section 6 we analyze the robot workspace, while Section 7 provides a brief mechanical description of the prototype and presents the first experimental results.

2. The modular architecture

Cheope has a hybrid kinematic structure composed of a "base movable points" Parallel Kinematic Machine (PKM) carrying on the mobile platform a serial chain $\underline{R}\,\underline{R}\,\underline{P}$ (see Fig. 1). The R and P denote a revolute and a prismatic joint, respectively, and the underscoring "_" means the joint is actuated. The parallel architecture is composed of 4 actuated prismatic joints (linear motors) set on the edges of a square pyramidal base (see Fig. 2). Each motor can be connected to the mobile base by a mechanical chain, or "leg", of 1 or 2 identical rods with a spherical joint at each end. The number and disposition of the rods can be reconfigured with simple and fast mechanical operations.

Each possible configuration is identified by a label indicating the sequence of joints for each "leg" and a subscript specifying the number of connecting rods between the linear motors and the mobile base. Fig. 3 shows a classification of the possible topological configurations:

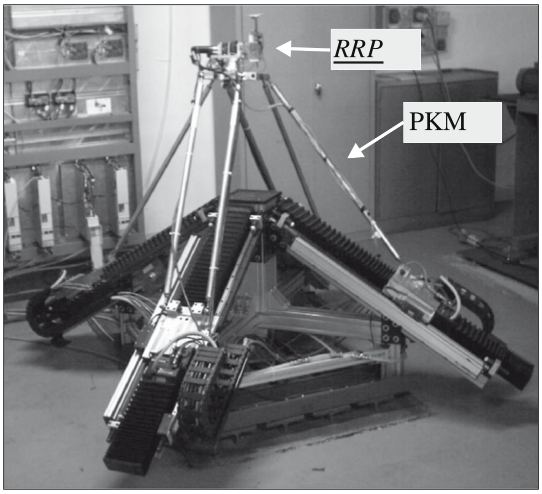

Fig. 1. The *Cheope* manipulator.

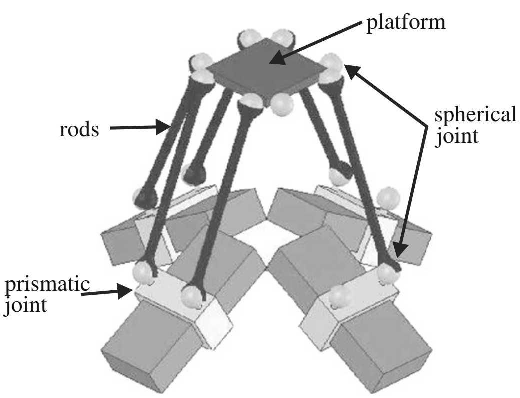

Fig. 2. Parallel kinematic structure.

Please cite this article in press as: D. Tosi et al., Cheope: A new reconfigurable redundant manipulator, Mech. Mach. Theory (2009), doi:10.1016/j.mechmachtheory.2009.11.005

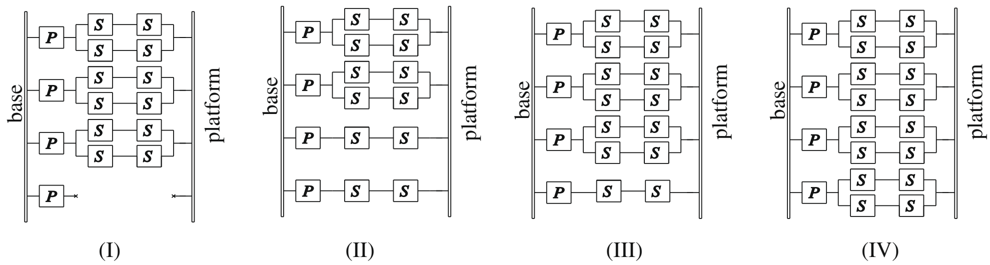

Fig. 3. Topological configurations of the parallel kinematic structure.

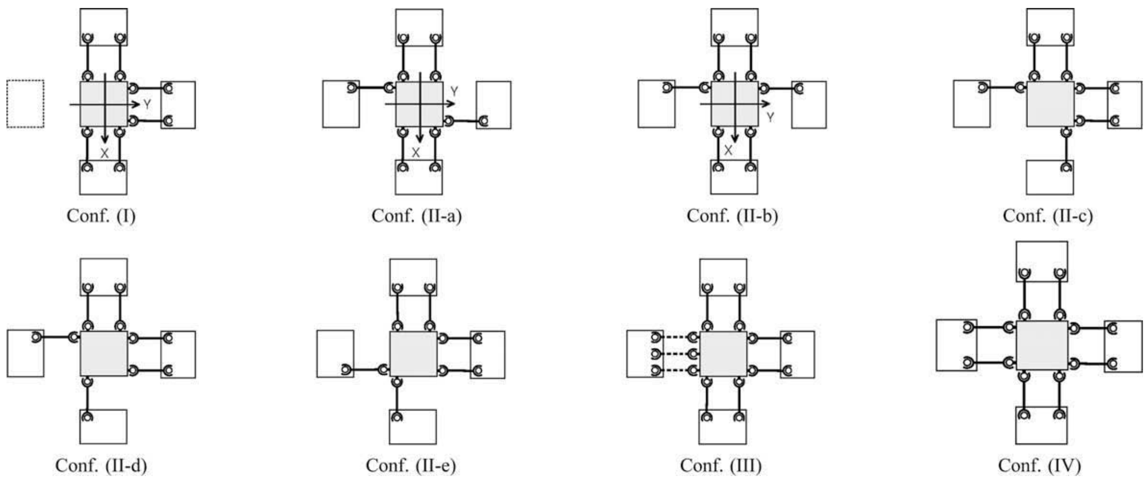

Fig. 4. The possible isostatic (I and II) and redundant configurations (III and IV).

(I) Three $\underline{P}[SS]_2$ legs (6 rods, 3 motors): the mobile base has 3 dof which correspond to a pure 3D-translation [12]; the fourth motor is not used.
(II) Two $\underline{P}[SS]_2$ and two $\underline{P}[SS]$ legs (6 rods, 4 motors): the mobile base has 4 dof which correspond to a 3D-translation and a rotation [11].
(III) Three $\underline{P}[SS]_2$ legs and one $\underline{P}[SS]$ leg (7 rods, 4 motors): the system is redundant; however, if correctly controlled it can became over-constrained, the mobile platform achieves 3 dof which correspond only to a pure 3D-translation.
(IV) Four $\underline{P}[SS]_2$ legs (8 rods, 4 motors): the mobility of the mobile platform is the same as the configuration (III).

Fig. 4 presents an overhead view of all the different configurations where the case labeled (II) is split in 5 sub-cases all having 4 dof, but different mobility characteristics.

In configuration (I) only 3 prismatic joints are actuated, and each of them is connected to the mobile base by a pair of rods. For the chosen geometrical dimensions, the rods of each pair are always parallel to each other and the mobile base can only translate within the workspace; no rotations are possible. If we limit our mobility study to first order kinematics [14] we observe that when the centers of the four spherical joints of each $\underline{P}[SS]_2$ leg lie in a plane (planar parallelogram); virtual rotations of the mobile base around any axis orthogonal to parallelogram plane are impossible. As the three pairs of legs lie in three different and linearly independent planes, all rotational directions are prevented (the end-effector can only translate).

Configurations (II-a) and (II-b) have 4 dof and the presence of two opposite pairs of rods prevents rotation of the mobile base about any axis that lies in the XZ plane. It can rotate around the Y axis and translate in X, Y and Z directions. Configurations (II-c), (II-d) and (II-e) have 4 dof as well; therefore the orientation of the rotation axis depends on the position of the mobile base, making these configurations less interesting.

Finally, the redundant configurations (III) and (IV) have 7 and 8 rods respectively, and the mobility of the base is the same as that of configuration (I) (pure 3D-translation). For the configuration (III) the 7th rod may be installed in any position shown by the three short dashed lines in the figure. The additional rods introduce internal constraints in the actuation of the prismatic joints (3 dof are controlled using 4 motors), and this can be conveniently used to improve the robot's performance in proximity of the singular configurations and compensate mechanical backlashes, as discussed in Section 5.

Additional assembly versions can be generated considering the configurations I, II, III, or IV and assembly one or more rods in an "central" intermediate position with respect the two indicated for each motors.

Please cite this article in press as: D. Tosi et al., Cheope: A new reconfigurable redundant manipulator, Mech. Mach. Theory (2009), doi:10.1016/j.mechmachtheory.2009.11.005

In this paper we focus only on configurations (I), (II-b) and (III). We refer to them as the *3 dof configuration*, *4 dof configuration* and *redundant 3 dof configuration*, respectively.

3. Kinematics

3.1. Notation

The kinematic analysis presented in this section is based on the adopted conventions shown in Fig. 5:

- *Prismatic (linear) axis and rods indexes*: $j = 1, \dots, k$ identifies the joint prismatic axis ($k = 3$ in *3 dof configuration*, $k = 4$ in *4 dof* or *3 dof redundant configuration*), (overhead view, counter-clockwise), $i = 1, \dots, 2k$ identifies the rod.
- $\{0\}$ is the absolute frame whose axes are $X_0Y_0Z_0$. The origin is in the intersection of the mechanical axes of the prismatic joints, Z_0 is the vertical axis (coincident with the chassis symmetry axis), and X_0 is the horizontal axis in the direction of prismatic joint 1.
- l: The length of rods.
- $\mathbf{w}_j$: The unit vector of the rod (or pair of rods) connected to the jth prismatic joint.
- $\mathbf{n}_j$: The unit vector of the jth prismatic joints.
- α: The rotation of the mobile base around the Y axis (used only in the *4 dof configuration*).
- $\mathbf{q} = [q_1, \dots, q_k]^T$ the joint coordinate vector, for 3 or 4 actuator case (respectively, $k = 3, k = 4$).
- $\mathbf{s}_3 = [x, y, z]^T$: Tool Center Point (TCP) coordinate vector, for 3 dof configuration.
- $\mathbf{s}_4 = [x, y, z, \alpha]^T$: Moving platform coordinate vector, for 4 dof configuration.
- A_i and B_i: the coordinates of the two end points of the ith rod. If $i = 1, 3, 5, 7$ then $A_i = A_{j,l}$ and $B_i = B_{j,l}$, where the subscript j, l means it is the left-hand-side rod for the jth linear axis ($i = 2j - 1$). If $i = 2, 4, 6, 8$ then $A_i = A_{j,r}$ and $B_i = B_{j,r}$ where the subscript j, r means it is the right-hand-side rod for the jth linear axis ($i = 2j$); (see Fig. 5c–e).
- $\overline{A}_j = \frac{1}{2}(A_{j,l} + A_{j,r})$ and $\overline{B}_j = \frac{1}{2}(B_{j,l} + B_{j,r})$: mean point between the ends of a pair of adjacent rods (see Fig. 5c and d);
- $\mathbf{a}_j$, $\mathbf{b}_j$ and $\mathbf{d}_j$: vectors associated to the point $B_{j,r}$ (see Fig. 5c and d).
- $\mathbf{f}_{xyz} = [f_x, f_y, f_z]^T$: external forces applied in the center of the platform (mobile base).
- $\mathbf{t}_{xyz} = [c_x, c_y, c_z]^T$: external torques applied to the platform.

We adopt the classical definition for kinematics:

- Direct (or forward) Kinematics: is the evaluation of the motion of the mobile base or of the TCP (Tool Center Point) when the motion of the motors is known.
- Inverse Kinematics: is the evaluation of the motion of the motors producing a pre-defined motion of the mobile base (or of the TCP).

3.2. Three dof configuration analysis

In this configuration, (Fig. 3-(I)), the mobile base can only translate since the two rods connected to the same prismatic joint remain parallel to each other. The kinematic analysis is developed by writing 3 closure loop equations, one for each pair of adjacent rods.

The loop-closure equation for the jth limb can be written along a virtual central rod connecting points $\overline{A}_j$ and $\overline{B}_j$ (see Fig. 5c and d):

$$\mathbf{s}_3 + \mathbf{a}_j - l\mathbf{w}_j - q_j\mathbf{n}_j = 0 \quad j = 1, \dots, 3 \tag{1}$$

Defining $\mathbf{c}_j(q_j) = q_j\mathbf{n}_j - \mathbf{a}_j$, from Eq. (1) we have:

$$|\mathbf{s}_3|^2 - 2\mathbf{c}_j(q_j)^T\mathbf{s}_3 + |\mathbf{c}_j(q_j)|^2 = l^2 \quad j = 1, \dots, 3 \tag{2}$$

The set of the three Eq. (1) represents the intersection of 3 spheres; l is their radius and $\mathbf{c}_j(q_j)$ are their centers.

3.2.1. Direct kinematics

The positions q_j of the motors are known; $\mathbf{s}_3$ (the mobile base position) must be determined. Since the position of the motors is known, the position of the spherical joints $\mathbf{c}_j(q_j)$ it is also known. To simplify the quadratic system we define the auxiliary frame {a} in which the equations of the spheres are simpler than in the absolute one. Frame {a} has origin O_a coincident with $\mathbf{c}_1, X_a$ passing trough $\mathbf{c}_2$ and the plane X_aY_a contains $\mathbf{c}_3$. In this frame the centers of the spheres are $\mathbf{c}_1 = [0, 0, 0]^T$, $\mathbf{c}_2 = [x_{c2}, 0, 0]^T$, $\mathbf{c}_3 = [x_{c3}, y_{c3}, 0]^T$. We indicate with $\mathbf{s}_a = [x_a, y_a, z_a]^T$ the intersection point of the three spheres expressed in frame {a}. The base position $\mathbf{s}_3$ can be computed from the product between the homogeneous transformation matrix $\mathbf{M}_{0a}$ (from frame {0} to {a}) and $\mathbf{s}_a$:

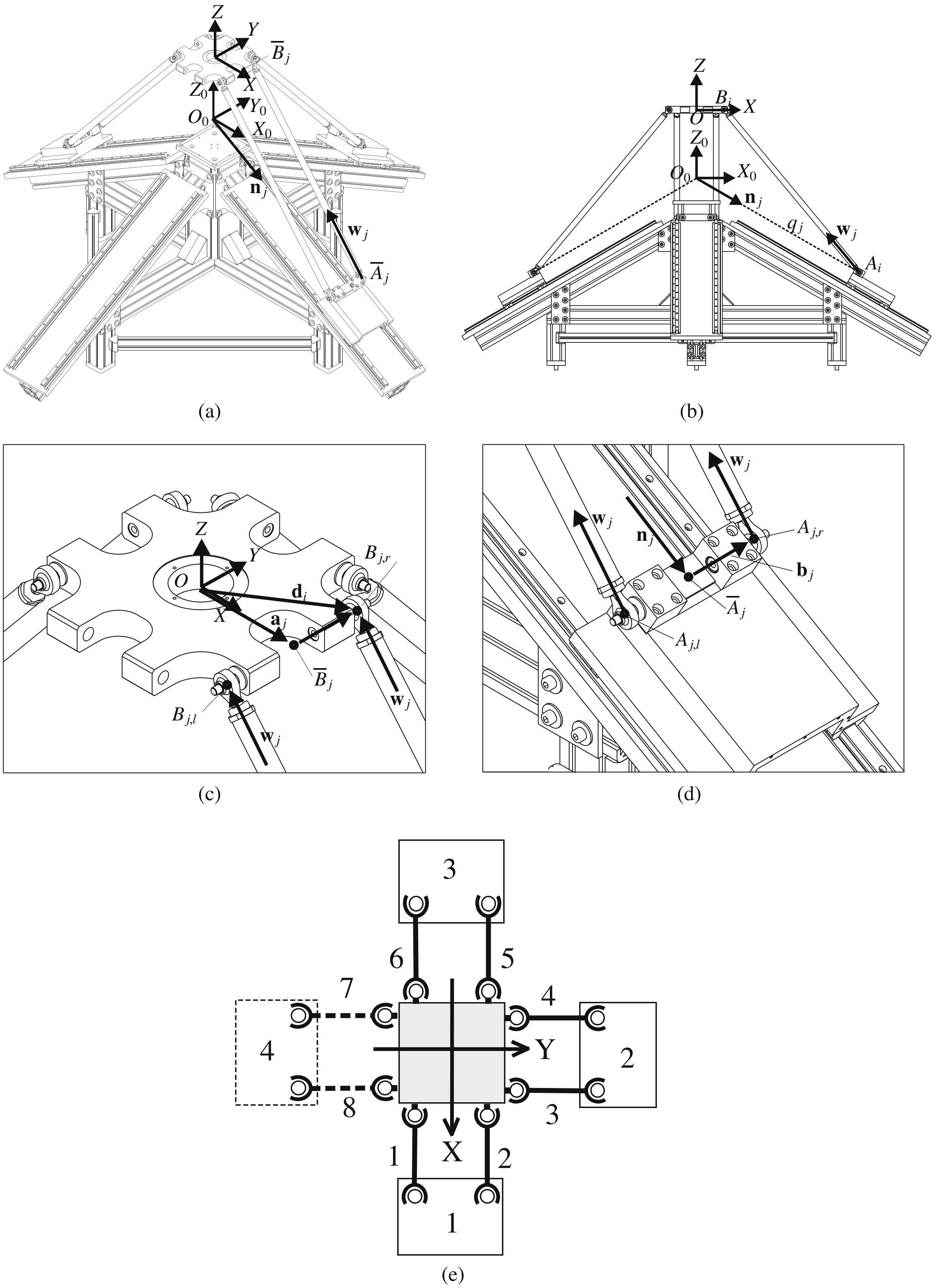

Fig. 5. The adopted notation.

Please cite this article in press as: D. Tosi et al., Cheope: A new reconfigurable redundant manipulator, Mech. Mach. Theory (2009), doi:10.1016/j.mechmachtheory.2009.11.005

$$\begin{bmatrix} \mathbf{s}_3 \\ \hline 1 \end{bmatrix} = \mathbf{M}_{0a}\mathbf{s}_a = \mathbf{M}_{0a}\begin{bmatrix} x_a \\ y_a \\ z_a \\ \hline 1 \end{bmatrix} \tag{3}$$

where

$$\mathbf{M}_{0a} = \left[\begin{array}{ccc|c} \frac{\mathbf{c}_2-\mathbf{c}_1}{|\mathbf{c}_2-\mathbf{c}_1|} & \frac{((\mathbf{c}_2-\mathbf{c}_1)\times(\mathbf{c}_3-\mathbf{c}_1))\times(\mathbf{c}_2-\mathbf{c}_1)}{|((\mathbf{c}_2-\mathbf{c}_1)\times(\mathbf{c}_3-\mathbf{c}_1))\times(\mathbf{c}_2-\mathbf{c}_1)|} & \frac{(\mathbf{c}_2-\mathbf{c}_1)\times(\mathbf{c}_3-\mathbf{c}_1)}{|(\mathbf{c}_2-\mathbf{c}_1)\times(\mathbf{c}_3-\mathbf{c}_1)|} & \mathbf{c}_1 \\ \hline 0 & 0 & 0 & 1 \end{array}\right] \tag{4}$$

where $\mathbf{c}_1, \mathbf{c}_2$, and $\mathbf{c}_3$ should be expressed in frame {0}.

Solving the system, we obtain two solutions, but only the one with the greater value for z is feasible because of the mechanical constraints of the robot. The other is not acceptable because it corresponds to a TCP (Tool Center Point) position within the manipulator base; $\mathbf{s}_a$ then is:

$$\begin{cases} x_a = x_{c2}/2 \\ y_a = (x_{c3}^2 + y_{c3}^2 - x_{c2}x_{c3})/(2y_{c3}) \\ z_a = \sqrt{l^2 - x_a^2 - y_a^2} \end{cases} \tag{5}$$

3.2.2. Inverse kinematics

The position $\mathbf{s}_3$ of the TCP is known; the positions q_j of the motor must be determined. The solution of this problem is simple as the three relations of Eq. (1) are uncoupled. Defining $\mathbf{r}_j = \mathbf{s}_3 + \mathbf{a}_j$ we have:

$$q_j = \mathbf{n}_j^T\mathbf{r}_j \pm \sqrt{(\mathbf{n}_j^T\mathbf{r}_j)^2 - \mathbf{r}_j^T\mathbf{r}_j + l^2} \quad j = 1, \ldots, 3 \tag{6}$$

Due to the mechanical limits only the solution with a positive sign before the radical can be accepted. The velocity and kinetostatic analysis require knowledge of Jacobian matrix. This is obtained with simple algebraic operations. Deriving Eq. (1) with respect to the time, we have:

$$\dot{\mathbf{s}}_3 - \dot{q}_j\mathbf{n}_j = l\omega_j \times \mathbf{w}_j \quad j = 1, \ldots, 3 \quad \text{with} \quad \frac{d}{dt}\mathbf{w}_j = \omega_j \times \mathbf{w}_j$$

where ω_j is the angular velocity of the jth rod. Projecting each equation on the rod direction $\mathbf{w}_j$, we have the relation that describes the inextensibility of the connection rods:

$$\mathbf{w}_j^T(\dot{\mathbf{s}}_3 - \dot{q}_j\mathbf{n}_j) = 0, \quad j = 1, \ldots, 3$$

By denoting as $\mathbf{W}_3$ and $\mathbf{K}_3$ the matrices

$$\mathbf{W}_3 = [\mathbf{w}_1\mathbf{w}_2\mathbf{w}_3], \quad \mathbf{K}_3 = \mathrm{diag}(\mathbf{w}_1^T\mathbf{n}_1, \mathbf{w}_2^T\mathbf{n}_2, \mathbf{w}_3^T\mathbf{n}_3) \tag{7}$$

the jacobian matrix $\mathbf{J}$ results:

$$\mathbf{W}_3^T\dot{\mathbf{s}}_3 = \mathbf{K}_3\dot{\mathbf{q}}, \quad \dot{\mathbf{q}} = \mathbf{J}\dot{\mathbf{s}}_3 \;\rightarrow\; \mathbf{J} = \mathbf{K}_3^{-1}\mathbf{W}_3^T \tag{8}$$

3.3. Four dof configuration analysis

In the 4 dof configuration the mobile base can rotate around the Y axis. The loop-closure equations are given by:

$$\begin{cases} \mathbf{s}_3 + \mathbf{a}_j(\alpha) - l\mathbf{w}_j - q_j\mathbf{n}_j = 0 & j = 1, 3 \\ \mathbf{s}_3 + \mathbf{d}_j(\alpha) - l\mathbf{w}_j - \mathbf{b}_j - q_j\mathbf{n}_j = 0 & j = 2, 4 \end{cases} \tag{9}$$

or, in a more compact form

$$\mathbf{s}_3 + \mathbf{k}_j(\alpha) - l\mathbf{w}_j - q_j\mathbf{n}_j = 0 \quad j = 1, \ldots, 4 \tag{10}$$

where

$$\mathbf{k}_j(\alpha) = \begin{cases} \mathbf{a}_j(\alpha) & j = 1, 3 \\ \mathbf{d}_j(\alpha) - \mathbf{b}_j & j = 2, 4 \end{cases} \tag{11}$$

3.3.1. Direct kinematics

The evaluation of $\mathbf{s}_4$ knowing q_j requires evaluation of the point of intersection of 4 spheres parametric in α. As analytical solution could not be found, a numerical procedure is implemented. To speed up the numerical solution for the run-time control of the robot, we have developed an algorithm based on a system reduction (from 4 to 2 equations) which is solved using the Newton–Raphson iterative method. To guarantee numerical convergence to the exact solution, the iterations are initialized using an approximate closed-form solution. Convergence was confirmed by extensive numerical tests.

3.3.2. Inverse kinematics

The inverse kinematics is similar to that of the 3 dof case. Defining $\mathbf{r}_j = \mathbf{s}_3 + \mathbf{k}_j$ we obtain:

$$q_j = \mathbf{n}_j^T\mathbf{r}_j + \sqrt{(\mathbf{n}_j^T\mathbf{r}_j)^2 - \mathbf{r}_j^T\mathbf{r}_j + l^2} \quad j = 1,\ldots,4$$

To complete the first order kinematic analysis, we compute the Jacobian matrix. Deriving Eq. (10) and projecting it in the rod direction $\mathbf{w}_j$, we have:

$$\dot{\mathbf{s}}_3 + \frac{d\mathbf{k}_j}{d\alpha}\dot{\alpha} - \dot{q}_j\mathbf{n}_j = l\omega_j \times \mathbf{w}_j \;\rightarrow\; \mathbf{w}_j^T\left(\dot{\mathbf{s}}_3 + \frac{d\mathbf{k}_j}{d\alpha}\dot{\alpha} - \dot{q}_j\mathbf{n}_j\right) = 0 \quad j = 1,\ldots,4 \tag{12}$$

Denoting as $\mathbf{W}_4$ and $\mathbf{K}_4$ the matrices

$$\mathbf{W}_4 = \begin{bmatrix} \mathbf{w}_1 & \mathbf{w}_2 & \mathbf{w}_3 & \mathbf{w}_4 \\ \mathbf{w}_1^T\frac{d\mathbf{k}_1}{d\alpha} & \mathbf{w}_2^T\frac{d\mathbf{k}_2}{d\alpha} & \mathbf{w}_3^T\frac{d\mathbf{k}_3}{d\alpha} & \mathbf{w}_4^T\frac{d\mathbf{k}_4}{d\alpha} \end{bmatrix} \quad \mathbf{K}_4 = \begin{bmatrix} \mathbf{w}_1^T\mathbf{n}_1 & 0 & 0 & 0 \\ 0 & \mathbf{w}_2^T\mathbf{n}_2 & 0 & 0 \\ 0 & 0 & \mathbf{w}_3^T\mathbf{n}_3 & 0 \\ 0 & 0 & 0 & \mathbf{w}_4^T\mathbf{n}_4 \end{bmatrix}$$

we have:

$$\mathbf{W}_4^T\dot{\mathbf{s}}_4 = \mathbf{K}_4\dot{\mathbf{q}} \;\rightarrow\; \mathbf{J} = \mathbf{K}_4^{-1}\mathbf{W}_4^T \tag{13}$$

4. Singularities analysis

4.1. Basic definitions

In designing the kinematic structure of the robot "Cheope" we have taken into account the working volume specifications and considered all the possible singularities; therefore the design process has led to confine the singular configurations outside the workspace, so that they are not achievable with the designed prismatic joints' mechanical stroke.

However, even when the manipulator is simply near a singular position, its performance indexes decrease very quickly (low stiffness, oscillations, difficult control optimization etc.).

Consequently, an accurate analysis of the singularities is imperative for the effective control. For a general robot the equation to develop position analysis can be written in the form $F(\mathbf{s}, \mathbf{q}) = 0$, and deriving with respect to time we have:

$$\mathbf{J}_s\dot{\mathbf{s}} = \mathbf{J}_q\dot{\mathbf{q}} \quad \text{with} \quad \mathbf{J}_s = \frac{\partial F}{\partial \mathbf{s}} \quad \text{and} \quad \mathbf{J}_q = -\frac{\partial F}{\partial \mathbf{q}} \tag{14}$$

Following the singularities analysis for parallel robots presented in [15] and more extensively in Zlatanov [17], the singular configuration for a generic robot arm can be classified as:

(a) *Direct Kinematic Singularity*: mathematically $\det(\mathbf{J}_s) = 0$ or $\det(\mathbf{J}_q) \rightarrow \infty$. This means that there is at least one vector $\dot{\mathbf{s}} \neq 0$ that gives $\dot{\mathbf{q}} = 0$. The mobile base gains one or more dof.

(b) *Inverse Kinematic Singularity*: mathematically $\det(\mathbf{J}_q) = 0$ or $\det(\mathbf{J}_s) \rightarrow \infty$. This means that there is at least one vector $\dot{\mathbf{q}} \neq 0$ that gives $\dot{\mathbf{s}} = 0$. The mobile base loses one or more dof.

(c) *Structural Singularity*: both the above conditions present; the manipulator is in a critical configuration where the structure may collapse.
Furthermore, in a non redundant-parallel manipulator with $n < 6$ degrees of freedom, the Jacobian matrix does not describe the system completely. For these manipulators, the structure transmits to the actuator only n external generalized forces (forces and torques) corresponding to the n degrees of freedom of the mobile base; the internal constraints balance any other forces applied on the end-effector. Therefore we can divide the 6-dimensional space of the generalized forces into two subspaces: we indicate with $\mathbf{f}_s$ the generalized forces balanced by the actuators and with $\mathbf{f}_c$ those balanced by the mechanical constraints. In agreement with [16], we consider an additional singularity configuration:

(d) *Constraint Singularity*: at least one $\mathbf{f}_c$ applied to the end-effector cannot be balanced by the internal constraints (a more detailed explanation is given in [18]).

The mobile base gains one or more uncontrollable dof, e.g the mobile base of a translational PKM gains a rotational dof (not described by the Jacobian matrix).

4.2. Three dof configuration singularities analysis

From Eqs. (7) and (8) we can write:

$$\begin{aligned} \det(\mathbf{J}_s) &= \det(\mathbf{W}_3) = \det(\mathbf{W}_3^T) = (\mathbf{w}_1 \times \mathbf{w}_2)^T\mathbf{w}_3 \\ \det(\mathbf{J}_q) &= \det(\mathbf{K}_3) = (\mathbf{w}_1^T\mathbf{n}_1)(\mathbf{w}_2^T\mathbf{n}_2)(\mathbf{w}_3^T\mathbf{n}_3) \end{aligned} \tag{15}$$

Please cite this article in press as: D. Tosi et al., Cheope: A new reconfigurable redundant manipulator, Mech. Mach. Theory (2009), doi:10.1016/j.mechmachtheory.2009.11.005

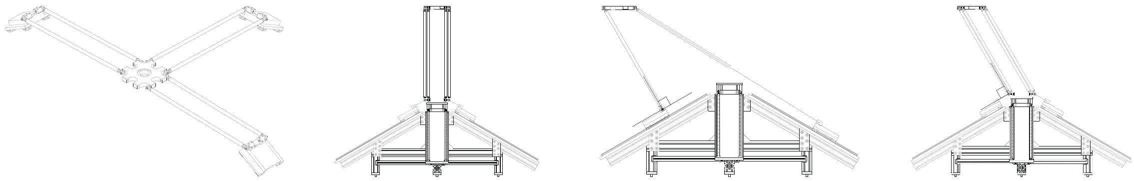

(a) (b) (c) (d)

Fig. 6. Singular configurations: from direct kinematic (a and b), from inverse kinematic (c) structural kinematic (d) for 3 dof configuration.

4.2.1. Direct kinematic singularities

These singularities occur when $\det(\mathbf{J}_s) = 0$, i.e. vectors $\mathbf{w}_j$ are linear dependent. Fig. 6a shows the case in which all the rods lie in the same plane, Fig. 6b shows the case in which two pairs of rods are parallel. In the first configuration, the mobile base can have an infinitesimal translation in Z direction, in the second it can reach finite translations in X and Y directions.

4.2.2. Inverse kinematic singularities

These singularities occur when $\det(\mathbf{J}_q) = 0$, i.e., at least one connecting rod is orthogonal to its prismatic axis joint (see Fig. 6c). The velocity of the mobile base in the rod direction is null.

4.2.3. Structural kinematic singularities

These singularities occur when both direct and inverse kinematic singularity is reached. An example is reported in Fig. 6d, where one pair of rods are orthogonal to one prismatic joint axis two (inverse kinematic singularity) and two pairs of rods are parallel to each other (direct kinematic singularity).

4.2.4. Constraint singularities

These singularities are detected by analyzing the relation between external generalized forces and internal (axial) forces transmitted to the mobile base by the connecting rods. The force transmitted by the ith rod can be expressed as the product of the force module and the rod unit vector:

$$\mathbf{f}_{ai} = f_{ai}\mathbf{w}_j \quad \text{with} \quad i = 1, \ldots, 6 \quad \text{and} \quad j = 1, \ldots, 3 \tag{16}$$

We can then indicate the vector of the axial forces in the rods as

$$\mathbf{f}_a = [f_{a1}, \ldots, f_{ai}, \ldots, f_{a6}]^T \tag{17}$$

and the forces and torques applied to the mobile base as

$$\mathbf{f}_s = \mathbf{f}_{xyz} = [f_x, f_y, f_z]^T \quad \mathbf{f}_t = \mathbf{t}_{xyz} = [t_x, t_y, t_z]^T \tag{18}$$

The relations between the external generalized forces and those at the rods can be obtained by examining the static equilibrium of the mobile base. In matrix form we can write

$$\begin{bmatrix} \mathbf{f}_s \\ \mathbf{f}_t \end{bmatrix} = \begin{bmatrix} \mathbf{W}_3 & 0 \\ \mathbf{W}_{a3} & \mathbf{W}_{b3} \end{bmatrix} \mathbf{T}_3 \mathbf{f}_a \quad \text{or} \quad \mathbf{T}_3 \mathbf{f}_a = \begin{bmatrix} \mathbf{W}_3^{-1} & 0 \\ -\mathbf{W}_{b3}^{-1}\mathbf{W}_{a3}\mathbf{W}^{-1} & \mathbf{W}_{b3}^{-1} \end{bmatrix} \begin{bmatrix} \mathbf{f}_s \\ \mathbf{f}_t \end{bmatrix} \tag{19}$$

where

$$\begin{aligned} \mathbf{W}_3 &= [\mathbf{w}_1 \ \ \mathbf{w}_2 \ \ \mathbf{w}_3] \\ \mathbf{W}_{a3} &= [\mathbf{w}_1 \times \mathbf{a}_1 \ \ \mathbf{w}_2 \times \mathbf{a}_2 \ \ \mathbf{w}_3 \times \mathbf{a}_3], \\ \mathbf{W}_{b3} &= [\mathbf{w}_1 \times \mathbf{b}_1 \ \ \mathbf{w}_2 \times \mathbf{b}_2 \ \ \mathbf{w}_3 \times \mathbf{b}_3] \end{aligned} \quad \mathbf{T}_3 = \begin{bmatrix} \overline{\mathbf{T}}_3 \\ \underline{\mathbf{T}}_3 \end{bmatrix} = \left[\begin{array}{cccccc} 1 & 1 & 0 & 0 & 0 & 0 \\ 0 & 0 & 1 & 1 & 0 & 0 \\ 0 & 0 & 0 & 0 & 1 & 1 \\ \hline -1 & 1 & 0 & 0 & 0 & 0 \\ 0 & 0 & -1 & 1 & 0 & 0 \\ 0 & 0 & 0 & 0 & -1 & 1 \end{array}\right]$$

Following [16], we must diagonalize the system of Eq. (19) to separate the influence of $\mathbf{f}_s$ and $\mathbf{f}_t$ from the internal rods forces $\mathbf{f}_a$:

$$\begin{bmatrix} \mathbb{I} & 0 \\ \mathbf{W}_{b3}^{-1}\mathbf{W}_{a3} & \mathbb{I} \end{bmatrix} \mathbf{T}_3 \mathbf{f}_a = \begin{bmatrix} \mathbf{W}_3^{-1} & 0 \\ 0 & \mathbf{W}_{b3}^{-1} \end{bmatrix} \begin{bmatrix} \mathbf{f}_s \\ \mathbf{f}_t \end{bmatrix} \tag{20}$$

where $\mathbb{I}$ is the identity matrix.

$$\begin{bmatrix} \mathbf{f}_s = \mathbf{W}_3 \overline{\mathbf{T}}_3 \mathbf{f}_a \\ \mathbf{f}_t = \mathbf{W}_{b3}\left(\mathbf{W}_{b3}^{-1}\mathbf{W}_{a3}\overline{\mathbf{T}}_3 + \underline{\mathbf{T}}_3\right)\mathbf{f}_a \end{bmatrix} \tag{21}$$

Please cite this article in press as: D. Tosi et al., Cheope: A new reconfigurable redundant manipulator, Mech. Mach. Theory (2009), doi:10.1016/j.mechmachtheory.2009.11.005

The constraint singularities are detected when $\det(\mathbf{W}_{b3}^{-1}) \to \infty$ or, equivalently $\det(\mathbf{W}_{b3}) = 0$. Considering the robot symmetries, we obtain the expression

$$\det(\mathbf{W}_{b3}) = -b^3 w_{2z}(w_{1z}w_{3x} - w_{1x}w_{3z}) \tag{22}$$

where b is the module of vector $\mathbf{b}_j$ and w_{ji} are the components of $\mathbf{w}_j$. Configurations of constraint singularly occur when:

- $b = 0$: the trivial case of coincident spherical joints;
- $w_{2z} = 0$: the second couple of rods are horizontal and the mobile base can rotate around Y-axis; this also occurs in the configuration of Fig. 6a.
- $w_{1z}w_{3x} = w_{1x}w_{3z}$: the projections of $\mathbf{w}_1$ and $\mathbf{w}_3$ on the X_0Z_0 plane are parallel to each other (this happens in coincidence of the direct kinematic singularity of Fig. 6a and b where the mobile base can rotate around the X and Z axes, respectively) or when the rods are orthogonal to X_0Z_0 plane.

4.3. Four dof configuration singularities analysis

Following the *3 dof configuration* approach, singular configurations occur when:

$$\begin{aligned}
\det(\mathbf{W}_4) &= \mathbf{w}_1^T \frac{d\mathbf{k}_1}{d\alpha}\left((\mathbf{w}_2 \times \mathbf{w}_3)^T \mathbf{w}_4\right) - \mathbf{w}_2^T \frac{d\mathbf{k}_2}{d\alpha}\left((\mathbf{w}_1 \times \mathbf{w}_3)^T \mathbf{w}_4\right) \\
&\quad + \mathbf{w}_3^T \frac{d\mathbf{k}_3}{d\alpha}\left((\mathbf{w}_1 \times \mathbf{w}_2)^T \mathbf{w}_4\right) - \mathbf{w}_4^T \frac{d\mathbf{k}_4}{d\alpha}\left((\mathbf{w}_1 \times \mathbf{w}_2)^T \mathbf{w}_3\right) = 0 \\
\det(\mathbf{K}_4) &= (\mathbf{w}_1^T\mathbf{n}_1)(\mathbf{w}_2^T\mathbf{n}_2)(\mathbf{w}_3^T\mathbf{n}_3)(\mathbf{w}_4^T\mathbf{n}_4) = 0
\end{aligned} \tag{23}$$

4.3.1. Direct, inverse and structural singularities

The same singularities of the *3 dof configuration* are present. Moreover, in each point of the workspace there are two mobile base rotation angles where the rods unit vectors $\mathbf{w}_j$ admit a common screw axis. When the center of the mobile base lies on the X_0Z_0 plane the rototranslation axis coincides with Y_0 (Fig. 7).

4.3.2. Constraint singularities

We have

$$\begin{aligned}
\mathbf{f}_s &= [\mathbf{f}_{xyz}^T, \mathbf{t}_{xyz}^T\mathbf{e}_y]^T = [f_x, f_y, f_z, t_y]^T \\
\mathbf{f}_t &= [\mathbf{t}_{xyz}^T\mathbf{e}_x, \mathbf{t}_{xyz}^T\mathbf{e}_z]^T = [t_x, t_z]^T
\end{aligned} \tag{24}$$

where $\mathbf{e}_x, \mathbf{e}_y$ and $\mathbf{e}_z$ are the unit vectors of axes X, Y and Z, respectively. Introducing

$$\mathbf{W}_{a4} = \begin{bmatrix} -aw_{1y}S_\alpha & bw_{2y}S_\alpha - aw_{2z} & aw_{1y}S_\alpha & bw_{4y}S_\alpha + aw_{4z} \\ -aw_{1y}C_\alpha & aw_{2x} + bw_{2y}C_\alpha & aw_{1y}C_\alpha & aw_{2x} + bw_{4y}C_\alpha \end{bmatrix}$$

$$\mathbf{W}_{b4} = \begin{bmatrix} 2bw_{1z} & -2bw_{3z} \\ -2bw_{1x} & 2bw_{3x} \end{bmatrix} \quad \mathbf{T}_4 = \begin{bmatrix} 1 & 1 & 0 & 0 & 0 & 0 \\ 0 & 0 & 1 & 0 & 0 & 0 \\ 0 & 0 & 0 & 1 & 1 & 0 \\ 0 & 0 & 0 & 0 & 0 & 1 \\ -1 & 1 & 0 & 0 & 0 & 0 \\ 0 & 0 & 0 & -1 & 1 & 0 \end{bmatrix}$$

where C_α and S_α are the sine and the cosine of α.

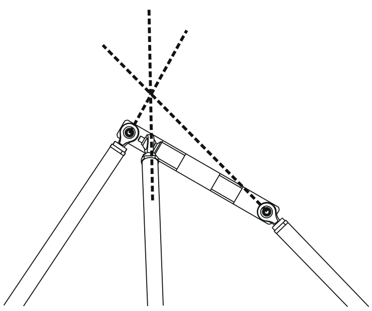

Fig. 7. Additional singular configuration for the 4 dof configuration.

Please cite this article in press as: D. Tosi et al., Cheope: A new reconfigurable redundant manipulator, Mech. Mach. Theory (2009), doi:10.1016/j.mechmachtheory.2009.11.005

we can write:

$$\begin{bmatrix} \mathbf{f}_{s4} \\ \mathbf{f}_{t4} \end{bmatrix} = \begin{bmatrix} \mathbf{W}_4 & 0 \\ \mathbf{W}_{a4} & \mathbf{W}_{b4} \end{bmatrix} \mathbf{T}_4 \mathbf{f}_{a4} \rightarrow \det(\mathbf{W}_{b4}) = b^2(w_{1z}w_{3x} - w_{1x}w_{3z}) \tag{25}$$

Therefore, the robot has a singular configuration if the projections of $\mathbf{w}_1$ and $\mathbf{w}_3$ on plane X_0Z_0 are parallel (or anti-parallel) to each other or if they are orthogonal to this plane.

5. Redundant three dof configuration

Repeatability is the measure of the dispersion of the pose reached by the end-effector when the manipulator is asked to move to the same pose several times in succession, and it is one of the most critical parameters for the performance of industrial manipulators. Poor repeatability is often caused by the mechanical clearance of the joints due to machining tolerances or wear phenomenons. Backlashes can also cause uncontrollable vibration during the robot's movements.

Besides the possibility of realizing expensive mechanical components of high accuracy, it is possible to compensate the effects of backlash by applying loads to the structure that can prevent the detachment of the coupled surfaces of the joints. Backlash is prevented if the force transmitted in each joint always has the same direction; otherwise, when the force inverts its direction the joint surfaces are free to detach, causing pose uncertainty and collisions.

Cheope has a redundant actuator [19] that can be conveniently used to apply an internal load to the moving part of the structure.

As shown in Fig. 4 configuration (III), a 7th redundant leg can be added in one of the three possible positions to the 3 dof configuration described here above. In this work the redundant leg has been installed in the middle position as shown in Fig. 8.

The redundant actuator can also be conveniently utilized to improve the robot performance in proximity of singular configurations (not discussed here).

Since backlash is prevented in the prismatic joints by the force of attraction of the linear motors, we shall consider only backlashes in the spherical joints which transmit the axial forces of the legs.

In order to simplify the notation, we can rename the elements of the vector of the axial forces Eq. (17) and reorder them in the new vector $\mathbf{f}'_a$ as follow

$$\mathbf{f}'_a = [f_{1,l},\ f_{2,l},\ f_{3,l},\ f_{1,r},\ f_{2,r},\ f_{3,r}]^T$$

where the subscripts indicate the number of the joint (to which the leg is connected) and the side of the rod (l: left-hand-side, r: right-hand-side).

The analysis requires the definition of the ratio between the axial force of the kth leg f'_{ak} and the force f_{q4} of the fourth (redundant) linear actuator (Fig. 8)

$$\tau_k = \frac{f'_{ak}}{f_{q4}} \quad k = 1, \ldots, 6$$

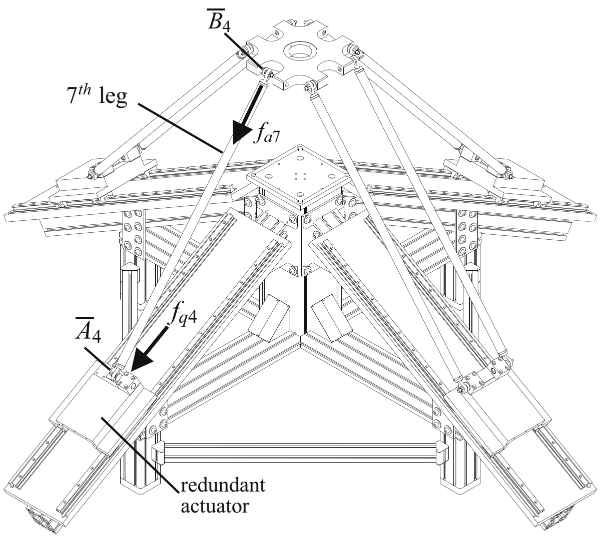

Fig. 8. Redundant configuration.

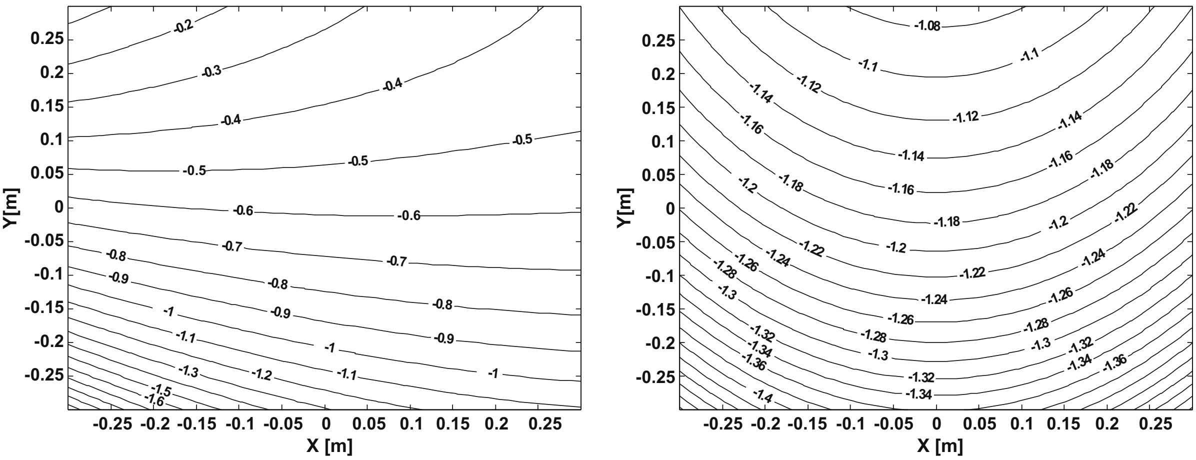

(a) (b)

Fig. 9. Values of τ_1 (a) and τ_7 (b) for $z = 0.5$ m.

In the case $\tau_k = 0$, the redundant actuator cannot exert any force in the kth leg. Furthermore, the sign of the τ_k ratios must remain constant in the entire workspace. Mathematically we write

$$|f_{q4}| < \frac{|f'_{ak}|}{\tau_{min}} \rightarrow |\tau_k| > \tau_{min} \quad k = 1, \ldots, 6$$

where τ_{min} is a suitable positive constant defined to prevent the redundant motor from generating excessive force in the first 6 legs. The seventh leg is considered separately, and defining f_{a7} as the axial force in the 7th leg (Fig. 8) we verify that in each point of the workspace

$$|\tau_7| = \left|\frac{f_{a7}}{f_{q4}}\right| = \frac{1}{\mathbf{w}_7^T \mathbf{n}_4} < \tau_{max} \tag{26}$$

where τ_{max} is a suitable constant assuring that the force of the 7th rod is limited. Using $\mathbf{f}'_a$ instead of $\mathbf{f}_a$, Eq. (19) becomes:

$$\begin{bmatrix} \mathbf{f}_{xyz} \\ \mathbf{t}_{xyz} \end{bmatrix} = \begin{bmatrix} \mathbf{W} & \mathbf{W} \\ \mathbf{W}_a + \mathbf{W}_b & \mathbf{W}_a - \mathbf{W}_b \end{bmatrix} \mathbf{f}'_a \tag{27}$$

where $\mathbf{f}_{xyz}$ and $\mathbf{t}_{xyz}$ are, respectively the forces and the torques applied to the mobile base that are balanced by $\mathbf{f}'_a$. Using the redundant leg to load the structure is equivalent to applying to the mobile base the following force:

$$\mathbf{f}_{xyz} = f_{a7}\mathbf{w}_7 \quad \mathbf{t}_{xyz} = f_{a7}\mathbf{w}_7 \times \mathbf{a}_4$$

Finally, we can calculate τ_k to estimate the influence of the 7th rod on the other ones. Using Eqs. (26) and (27) we can write

$$\boldsymbol{\tau} = [\,\tau_1 \quad \ldots, \quad \tau_k \quad, \ldots, \quad \tau_6\,]^T = \frac{1}{2\mathbf{w}_7^T \mathbf{n}_4} \begin{bmatrix} (\mathbb{I} - \mathbf{W}_b^{-1}\mathbf{W}_a)\mathbf{W}^{-1} & \mathbf{W}_b^{-1} \\ (\mathbb{I} + \mathbf{W}_b^{-1}\mathbf{W}_a)\mathbf{W}^{-1} & -\mathbf{W}_b^{-1} \end{bmatrix} \begin{bmatrix} \mathbf{w}_7 \\ \mathbf{w}_7 \times \mathbf{a}_4 \end{bmatrix}$$

Fig. 9 displays the results of simulations performed with the real geometrical dimensions of the prototype. Here we see that the elements of $\boldsymbol{\tau}$ keep the same sign and their values are far from zero in most of the workspace. The ratio τ_7 never exceeds the value of 2. This confirms the applicability of the proposed method of backlash compensation.

6. Workspace

In addition to the worsening of the kinetostatic performance in the proximity of the singular configurations, the workspace of the robot is limited by the endstops of the joints. The analysis of the limits imposed by the endstops of the prismatic joints of the actuators is quite simple (the workspace is obtained as an intersection of spheres), while the study of the spherical joints is more complex.

The legs of the robot have a spherical joint at each end. The rotation of the joint is limited by the interference of the external ring with the transversal pin keyed in the bore of the sphere (see Fig. 10). For the spherical joint used the pin can move inside a cone with a semi-aperture angle $\gamma = 22$ [deg]. For each pose of the mobile base, we must verify that none of the 12 spherical joints exceeds the rotation limits. The two spherical joints of each rod must be analyzed together. Each leg has a free dof of rotation about its axis and the external rings of the spherical joints with the “admitted cones” rotate with the leg.

Please cite this article in press as: D. Tosi et al., Cheope: A new reconfigurable redundant manipulator, Mech. Mach. Theory (2009), doi:10.1016/j.mechmachtheory.2009.11.005

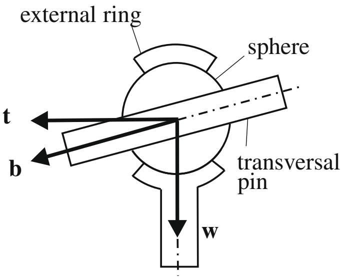

Fig. 10. A section of a spherical joint.

A pose is admissible if each leg can perform at least an angular rotation about its axis that satisfies the limits at both ends. We indicate with $\mathbf{t}$ the unit vector of the axis of the external ring which is orthogonal to the unit vector $\mathbf{w}$ of the leg and with $\mathbf{b}$ the unit vector of the pin axis (see Fig. 10). This axis always has a constant direction, excepts in the case of the joints of the mobile base in the 4 dof configuration. For a given pose of the mobile base with the corresponding direction of the pin we can write the following system which summarizes the constraints relation

$$\begin{cases} \mathbf{b}^T\mathbf{t} \geqslant \cos\gamma \\ \mathbf{w}^T\mathbf{t} = 0 \\ \mathbf{t}^T\mathbf{t} = 1 \end{cases}$$

On the boundary of the constraint sign "$\geqslant$" is replaced by an equal sign "=" and we obtain a system in the unknown $\mathbf{t} = [t_x t_y t_z]$.

We indicate by $\bar{\mathbf{t}}$ a unit vector in the plane defined by the two vectors $\mathbf{b}$ and $\mathbf{w}$. We then introduce the unit vector $\mathbf{k}$ such that it is normal to this plane and can be calculated as:

$$\mathbf{k} = \frac{\mathbf{w} \times \mathbf{b}}{\|\mathbf{w} \times \mathbf{b}\|}$$

The unit vector $\mathbf{t}$ can be expressed as:

$$\mathbf{t} = \lambda_t \bar{\mathbf{t}} + \lambda_k \mathbf{k}$$

where λ_t and λ_k are suitable scalars. In order to understand the physical meaning of the vector $\bar{\mathbf{t}}$, we hypothesize a leg rotating around its axis. The unit vector $\mathbf{t}$ can assume a direction between two boundary conditions, called $\mathbf{t}_1$ and $\mathbf{t}_2$; then $\bar{\mathbf{t}}$ is the mean value between them and can be easily determined by:

$$\bar{\mathbf{t}} = \frac{\mathbf{w} \times \mathbf{k}}{\|\mathbf{w} \times \mathbf{k}\|}$$

Once $\bar{\mathbf{t}}$ is determined, we can calculate the boundary solutions $\mathbf{t}_1$ and $\mathbf{t}_2$, by solving the following system:

$$\begin{bmatrix} \mathbf{t}^T \\ \mathbf{b}^T \end{bmatrix} \mathbf{t} = \begin{bmatrix} 1 \\ \cos\gamma \end{bmatrix} \rightarrow \begin{cases} \lambda_t^2 + \lambda_k^2 = 1 \\ \lambda_t \mathbf{b}^T \bar{\mathbf{t}} = \cos\gamma \end{cases}$$

Obtaining:

$$\mathbf{t}_1 = \frac{\cos\gamma}{\mathbf{b}^T\bar{\mathbf{t}}}\bar{\mathbf{t}} + \sqrt{1 - \left(\frac{\cos\gamma}{\mathbf{b}^T\bar{\mathbf{t}}}\right)^2}$$
$$\mathbf{t}_2 = \frac{\cos\gamma}{\mathbf{b}^T\bar{\mathbf{t}}}\bar{\mathbf{t}} - \sqrt{1 - \left(\frac{\cos\gamma}{\mathbf{b}^T\bar{\mathbf{t}}}\right)^2}$$

The described procedure must be applied to both ends of each leg computing the extreme directions $\{\mathbf{t}_{A1}\mathbf{t}_{A2}\}$ for the spherical joint of the mobile base and $\{\mathbf{t}_{B1}\mathbf{t}_{B2}\}$ for the prismatic one. Now we must verify the existence of an axial rotation of the leg that satisfies both intervals. This is equivalent to verifying the existence of the dark circular sector of Fig. 11. To prove this it is sufficient to verify that at least one of the four extreme directions is included between the two directions computed for the opposite end of the leg. Mathematically, for example, $\mathbf{t}_{A1}$ is included between $\mathbf{t}_{B1}$ and $\mathbf{t}_{B2}$ if

$$\mathbf{t}_{A1}^T\mathbf{t}_{B1} < \mathbf{t}_{B1}^T\mathbf{t}_{B2} \quad \text{and} \quad \mathbf{t}_{A1}^T\mathbf{t}_{B2} < \mathbf{t}_{B1}^T\mathbf{t}_{B2}$$

Fig. 12a and b represent some sections of the working space of the robot for the 3 dof and the 4 dof configurations numerically computed considering all joint limits. For the 4 dof configuration it is possible to compute the maximum and the minimum rotation, α_{max} and α_{min}, respectively, of the mobile base for each workspace position, as illustrated in Fig. 12c.

Please cite this article in press as: D. Tosi et al., Cheope: A new reconfigurable redundant manipulator, Mech. Mach. Theory (2009), doi:10.1016/j.mechmachtheory.2009.11.005

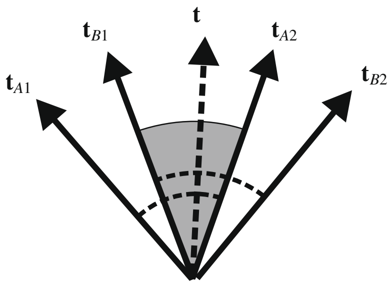

Fig. 11. The admitted motion for **t**.

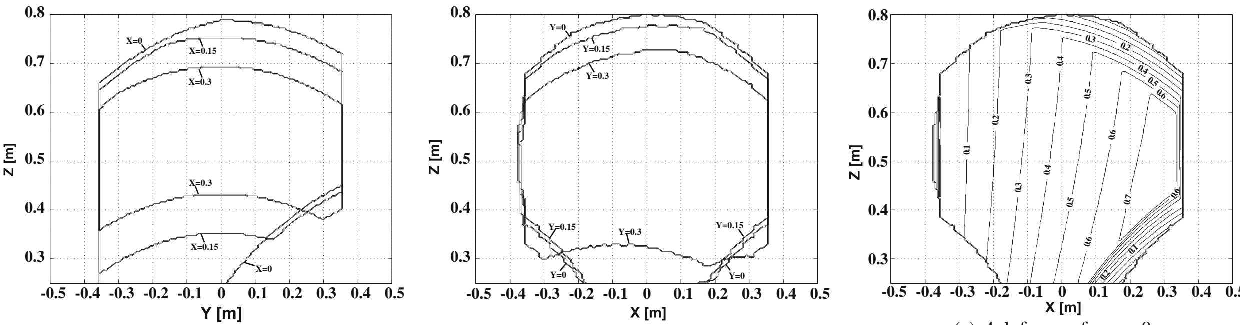

(a) 3 dof

(b) 4 dof

(c) 4 dof, α_{max} for $y = 0$

Fig. 12. Workspace limits.

Table 1
Geometrical dimensions and masses.

Slope of the prismatic joints (ψ)	30 deg	Mobile base	2 kg
Total cursors stroke	700 mm	Wrist mass	3 kg
Rod length (l)	950 mm	Rod mass	1 kg
Half-distance between sph. joints (b)	85 mm	Cursor mass	4 kg
Half-side of the mobile base (a)	120 mm		

7. Mechanical structure and performances

The geometrical dimensions and approximate masses of the Cheope manipulator, as designed, built and assembled in the context of the RIME project, are shown in Table 1.

The components used for the prismatic actuators play a role of primary importance in the manipulator's performances. Its parallel architecture utilizes four linear brushless motors with a continuous and a peak force of 240 N and 800 N, respectively. The maximum speed and acceleration of the cursors are limited to 2 m/s and 50 m/s^2, respectively by the optical linear transducers, which have an accuracy of ±5 μm.

Repeatability tests performed in different points of the workspace gave good results. Unidirectional tests provided a mean and a maximum error of 10.6 μm and 22.3 μm, respectively while in multidirectional tests the error values were 28.0 μm and 52.0 μm, respectively.

Two different sets of dynamic tests were developed for the 3 dof configuration (see Fig. 4-(I)):

- measure of the accelerations of the Tool Center Point (TCP) using the "Blue-Box measuring system" [20], (see Fig. 13);
- measure of the maximum performances using a tri-axial accelerometer.

7.1. First set of tests

The first set of experiments served to verify the precision of the mechanical assembly of the robot. The objectives here were two: verify that the motion of the mobile base of the parallel structure was exactly a 3D translation, and study the stiffness of the kinematic chain. The experimental set-up was composed of a cubic "Blue-Box", designed and equipped by the

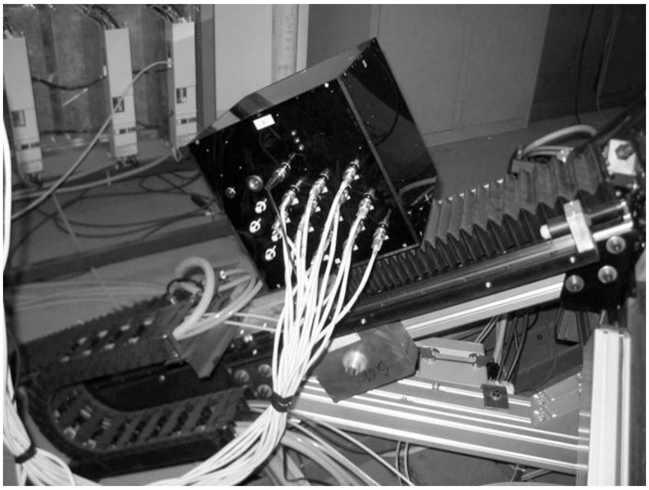

Fig. 13. First set of tests: measure of the single-slide acceleration.

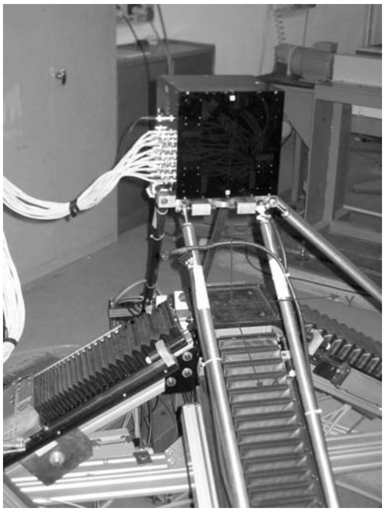

Fig. 14. First set of tests: measure of the mobile base accelerations.

Politecnico di Milano [20,21], with 4 tri-axial accelerometers in a non-singular configuration. It measures the 3 linear accelerations $a_x a_y a_z$, the 3 angular accelerations $\dot{\omega}_x \dot{\omega}_y \dot{\omega}_z$, and the values of the 3 angular velocities $\omega_x \omega_y \omega_z$ simultaneously. The maximum acceleration the Blue-Box can measure is equal to 10 m/s^2.

Two different experiments were developed in order to measure:

- the accelerations of the linear actuators;
- the accelerations of the mobile base of the parallel structure.

The first experiment is a forward-backward movement of 200 mm with a triangular velocity and a maximum acceleration of 10 m/s^2 (see Fig. 13). Fig. 15a compares the values of the acceleration measured by the Blue-Box with the theoretical one.

In the second experiment the BlueBox was fixed to the mobile platform (see Fig. 14). The mobile platform had to follow a circular trajectory with radius $r = 100$ mm and centered in $x_c = 0$ mm, $y_c = 0$ mm, $z_c = 500$ mm. Fig. 15b reports the comparison between the measured values of the accelerations and the theoretical ones.

The good agreement between the measured and the calculated acceleration confirms that the kinematic chain has a great stiffness and no backlashes, and that mobile base has a pure translational movements.

7.2. Second set of tests

The second set of tests was designed to measure the maximum performance of Cheope. The experimental set-up was composed simply of a tri-axial accelerometer with a range of measure of ±10 g, stiffly linked to the mobile platform. The

Please cite this article in press as: D. Tosi et al., Cheope: A new reconfigurable redundant manipulator, Mech. Mach. Theory (2009), doi:10.1016/j.mechmachtheory.2009.11.005

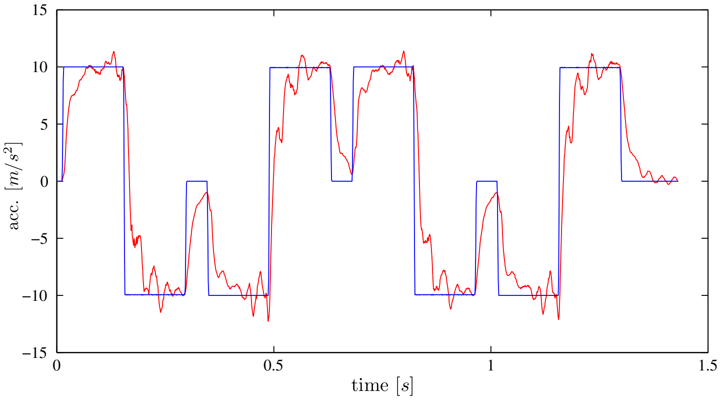

(a) 1-axis return movement: measured and theoretical acceleration

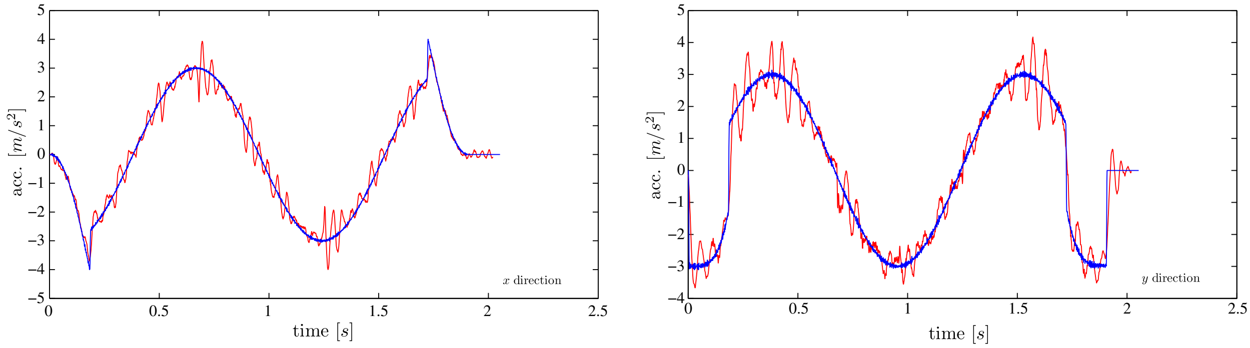

(b) coordinate movement: measured and theoretical acceleration

Fig. 15. First set of tests: analysis of the mechanical structure.

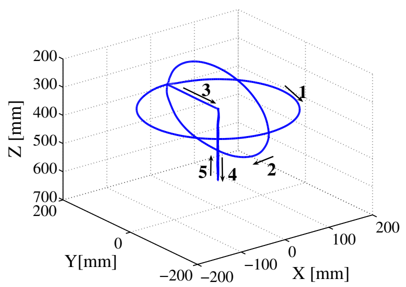

(a) Trajectory

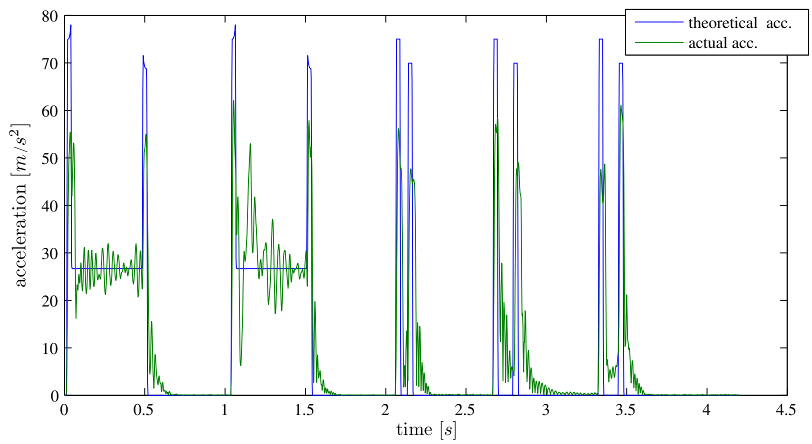

(b) acceleration

Fig. 16. Second set of tests: motion of the platform. Comparison between the theoretical acceleration and the measured one.

TCP had to follow the trajectory displayed in Fig. 16a, composed of two circles and three linear movements. Fig. 16b compares the module of the theoretical acceleration and measured one for the TCP. The acceleration oscillation at 1 s is due to the asymmetry of the structure (see Fig. 4-(I)): the circular movement required is on the *YZ*-plane and the movement along *Y* is controlled by only one actuator. When, instead, the TCP follows a circular trajectory in the *XZ*-plane, the movement is controlled by two actuators and there is no overshoot in the velocity profile. The picture shows that the TCP can reach an acceleration of 60 m/s^2.

Please cite this article in press as: D. Tosi et al., Cheope: A new reconfigurable redundant manipulator, Mech. Mach. Theory (2009), doi:10.1016/j.mechmachtheory.2009.11.005

8. Conclusions

All the main aspects of the kinematical characteristics of the Cheope manipulator have been presented. Direct and inverse kinematics have been developed and analytical expressions of the direct, inverse, structural and constraint singularities obtained. An applicability criterion for the elimination of joint backlash in the redundant actuated configuration has been proposed and verified. These results together with the analysis of the workspace, have ensured the design of a robot of satisfactory kinematic behavior. The choice of high performance mechanical components (mainly the linear motors) has produced an equally good dynamic response. Cheope, initially designed as a prototype for medical applications, can be conveniently applied in various other fields (machining, surface finishing, assembly tasks, etc).

References

[1] <http://www.intuitivesurgical.com/>.
[2] Intelligent System Report, vol. 16, No 10, November 1999.
[3] D. Tosi, G. Legnani, R. Adamini, H. Giberti, P. Righettini, Progetto di "CHEOPE": un manipolatore ridondante ibrido parallelo-seriale, in: AIMETA 2003, Ferrara, 9–12 Settembre 2003.
[4] L.W. Tsai, Robot Analysis: The Mechanics of Serial and Parallel Manipulators, Wiley, New York, 1999.
[5] F. Gao et al, New kinematic structures for 2-,3-,4- and 5-dof parallel manipulator designs, Mechanism and Machine Theory 37 (11) (2002) 1395–1411.
[6] R. Ricard, C.M. Gosselin, in: On the Development of Hybrid Planar Manipulators 6th IEEE Midwest Symposium on Circuits and Systems, Detroit, August 16–18, 1993.
[7] Tanio K. Tanev, Kinematics of a hybrid (parallel-serial) robot, Mechanism and Machine Theory 35 (2000) 1183–1196.
[8] Hyeun-Seok Choia, Chang-Soo Hana, Kye-Young Lee, Sang-Heon Lee, Development of hybrid robot for construction works with pneumatic actuator, Automation in Construction 14 (4) (2005) 452–459.
[9] T. Huang, D.J. Whitehouse, J. Wang, The local dexterity, Optimal Architecture and Design Criteria of Parallel Machine Tools, Annals of the CIRP, 47/1:347-351, 1998.
[10] J.M. Herve, F. Sparacino, Star, a new concept in robotics, in: 3rd International Workshop on Advances in Robot Kinematics, September 7–9, 1992, Ferrara, Italy, pp. 176–183.
[11] L. Rolland, The Manta and the Kanuk: Novel 4-DOF parallel mechanisms for industrial handling, in: Proceedings of the ASME Dynamic Systems and Control Division, IMECE'99 Conference, vol. 67, Nashville, USA, Nov. 14–19, 1999, pp. 831–844.
[12] M. Hebsacker, T. Treib, O. Zim, M. Honegger, Hexaglide 6 DOF and Triaglide 3 DOF parallel manipulators, in: C.R. Boer, L. Molinari-Tosatti, K.S. Smith (Eds.), Parallel Kinematic Machines: Theoretical Aspects and Industrial Requirements, Springer-Verlag, 1999, pp. 345–355.
[13] S. Krut, O. Company, M. Benoit, H. Ota, F. Pierrot, I4: a new parallel mechanism for scara motions, in: IEEE Rob. and Autom. Conf., Taipei, 2003.
[14] R.S. Ball, A Treatise on the Theory of Screws, Cambridge University Press, Cambridge, 1900.
[15] G. Legnani, Robotica Industriale, Editrice Ambrosiana, Milano, 2003.
[16] M. Zoppi, L. Bruzzone, R. Molfino, R. Michelini, Constraint singularities of force transmission in nonredundant parallel robots with less than six degrees of freedom, Transactions on ASME Journal of Mechanical Design 1 (2003) 1–2.
[17] D. Zlatanov, R.G. Fenton, B. Benhabib, Identification and classification of the singular configurations mechanism, Mechanism and Machine Theory 33 (6) (1998) 743–760;.
[18] D. Zlatanov, R.G. Fenton, B. Benhabib, Singularity analysis of mechanism and robots via a motion-space model of the instantaneous kinematics, in: Proceedings of the IEEE International Conference on Robotics and Automation, San Diego, CA, 1994, pp. 980–985.
[19] C. Reboulet, C. Lambert, N. Nombrail, A parallel redundant manipulator: SPEED-R-MAN and its control, in: 4th ISRAM, Santa-Fe, Nov. 11–13, 1992, pp. 285–291.
[20] M. Camposaragna, F. Casolo, B. Cattaneo, N. Baldo, Blue-box: a device to rebuild the 3D kinematics and the actions on the drivers along a road path, in: Congresso Internationale SIIV, Firenze, 27–29 Octobre 2004.
[21] M. Camposaragna, F. Casolo, M. Cocetta, "Un dispositivo per la misura di accelerazioni 3D per applicazioni in campo automobilistico" *Michele Camposaragna, Federico Casolo, Barbara Cattaneo, Simone Cinquemani, Giovanni Legnani*, XVII Congresso AIMETA di Meccanica Teorica e Applicata, Firenze 11–15 Settembre 2005.

Please cite this article in press as: D. Tosi et al., Cheope: A new reconfigurable redundant manipulator, Mech. Mach. Theory (2009), doi:10.1016/j.mechmachtheory.2009.11.005